water

MDPI

Article

Egg White Protein–Soybean Protein Isolate Hierarchical Network Hydrogel for Enhanced Adsorption of Methylene Blue

Mei Zhang and Xu Wang *

School of Materials Science and Engineering, Yancheng Institute of Technology, Yancheng 224051, China
* Correspondence: wangxu@ycit.cn

Abstract: In terms of environmental protection and the sustainable development of society, the constraint of dye concentrations in industrial wastewater is vitally important for the development of every country. In this study, egg white protein (EWP)–soybean protein isolate (SPI) hierarchical-network hydrogel beads reinforced with calcium alginate are devised using a one-step chemical crosslinking. The prepared EWP/SPI beads, with a specific surface area of 26.55 $m^2 \cdot g^{-1}$, possess a self-floating ability that enhances their solid–liquid separation of methylene blue (MB) from industrial sewage and achieves adsorption equilibrium within 60 min. The investigation of adsorption behavior indicates that the results fitted well with the Langmuir isotherm mode and pseudo-first-order kinetic model. Based on the pseudo-first-order kinetic model and the Langmuir model, the equilibrium adsorption capacity and maximum adsorption capacity of the EWP/SPI hydrogel beads towards MB are 187.495 and 336.265 $mg \cdot g^{-1}$, respectively. Furthermore, the favorable regeneration of the EWP/SPI hydrogel is demonstrated, with a removal efficiency towards MB decreasing from 94% to 82% (10 mg dose, 100 $mg \cdot L^{-1}$ MB, pH 7, 25 °C) after five adsorption–desorption cycles. The resulting EWP/SPI hydrogel beads with hydrophilicity exhibited good self-floating stability (above 80%) in wastewater for 7 days, suggesting their potential for recycling in diverse complex environments. Therefore, the inexpensive and sustainable floating EWP/SPI hydrogel beads provide a new insight for organic pollutant treatment in wastewater.

Keywords: egg white protein; soybean protein isolate; hydrogel; water treatment

Citation: Zhang, M.; Wang, X. Egg White Protein–Soybean Protein Isolate Hierarchical Network Hydrogel for Enhanced Adsorption of Methylene Blue. *Water* **2024**, *16*, 3357. https://doi.org/10.3390/w16233357

Academic Editor: Laura Bulgariu

Received: 30 October 2024
Revised: 17 November 2024
Accepted: 19 November 2024
Published: 22 November 2024

1. Introduction

With the rapid development of the textile industry, the utilization of dyes has dramatically increased [1]. Without proper treatment, these toxic and carcinogenic dyes will remain in soils and water bodies and accumulate in the body at various levels of the food chain for a long time in a manner that seriously threatens human health [2,3]. Therefore, the constraint of dye concentrations in industrial wastewater in the environment is extremely important [4,5]. In recent decades, a great many treatments have already been employed to remove various organic dye molecules, such as photodegradation [6–8], chemical oxidation [9], filtration [10,11], or adsorption [12–14]. Among all these treatments, adsorption is now considered an attractive approach due to its high adsorption efficiency, low cost, easy operation, and reusability. As a result, adsorption is widely used to alleviate the harm caused by organic dyes. However, the application of the adsorption method faces limits in terms of the low adsorption capability and inferior separation efficiency caused by the precipitation of traditional adsorbents to the bottom of the container, which reduces the contact between the adsorbent and the dye contaminants [15,16]. Consequently, devising an adsorbent that can remove dyes efficiently, coupled with environmental friendliness and an acceptable mechanical property of reusability, is still a challenging task.

Hydrogels with a three-dimensional (3D) network structure formed by the crosslinking of polymers exhibit an excellent dye removal ability due to their high specific surface area. In particular, a new generation of biomass-based hydrogels have attracted a lot of

attention as they are plentiful, inexpensive, sustainable, and biodegradable [17]. Numerous kinds of biomass-based hydrogels, including alginate, chitosan, starch, kaolinite, and cellulose, have been employed to remove pollutants containing organic dyes. Kalidhasan et al. synthesized soy lecithin (SL)–Au (LG) and SL-Au-Cu (LGC) catalysts efficiently and degraded rhodamine B (RB, 100%) in the presence of H_2O_2 under light irradiation [18]. Zhang et al. designed alginate/organo-selenium hydrogel beads for both dye adsorption and bacterial deactivation [19]. Sayyar et al. prepared a low-cost chitosan modified with a montmorillonite/ZnO hydrogel nanocomposite for the adsorption of ciprofloxacin from water [20]. In our country, the biomass-derived raw materials are based on abundant agricultural resources [21–23]. Among these natural resources, protein-based adsorbents are especially well received in different sectors due to their prominent properties, such as massive functional groups, biodegradability, biocompatibility, and lower toxicity compared with artificial synthetic polymers [24–27].

Egg white (EW) is a common material with multifunctional properties, such as gelling, heat setting, foaming, bonding, and emulsifying. As a result, EW is widely used as an ideal ingredient in the food industry. In view of the other advantages of EW, such as its low cost, multiple functions, sustainability, and, eco-friendliness, it has excellent prospects for applications in the preparation of new functional materials. Yan et al. constructed an egg white protein (EWP)–gallic acid–xanthan gum-based emulsion and oleogel [28]. Soy protein isolate (SPI) from soybean consists of about 20 different amino acids, such as lysine, aspartic, leucine, glutamic acid, and tyrosine. SPI with desirable functionalities has been widely applied in biodegradable material preparation. Moreover, SPI with positive chelating properties has been reported as an adsorbent for wastewater treatment. Revadekar et al. developed an SPI–sodium alginate-based aerogel for the efficient uptake of organic dye from effluents [29]. Lu et al. designed a double-crosslinked chitosan sponge encapsulated with ZrO_2–SPI amyloid fibril nanoparticles for the removal of fluoride ions from water [30].

In this study, we propose a novel approach to preparing an EWP/SPI hierarchical-network hydrogel reinforced with calcium alginate using a simultaneous one-step chemical crosslinking. In this hydrogel, the crosslinking of EWP forms the first-order network structure, and the crosslinking of SPI generates the second-order network structure. Alginates are added into hydrogels to build a third-order network and enhance the mechanical properties of hydrogels through crosslinking with Ca^{2+}. The synthesized hydrogel with a three-level network can be used as an adsorbent for the removal of organic dyes. The obtained experimental results indicate that the EWP/SPI hydrogel has a favorable adsorption capacity and adsorption efficiency for methylene blue.

2. Materials and Methods

2.1. Materials

Egg white protein (EWP), soybean protein isolate (SPI), sodium alginate (SA), calcium chloride anhydrous ($CaCl_2$), methylene blue (MB), glutaraldehyde, and hydrochloric acid (HCl) were provided by Sinopharm Chemical Reagent Co. Ltd., Shanghai, China. All experimental reagents were of analytical grade and could be used directly without further purification.

2.2. Preparation of EWP/SPI Hydrogel Beads

To prepare the EWP/SPI hydrogel beads, we firstly prepared an EWP/SPI/sodium alginate mixture. Briefly, 1.0 g SPI and 1.0 g EWP were added into 50.0 mL deionized water to form an EWP/SPI mixture [24,31,32]. Then, the mixture was strongly stirred for 30 min, followed by 20 min ultrasonication using an ultrasonic device with a power of 300 W to uniformly disperse the mixture. After that, the EWP/SPI mixture was added into an SA solution (1 wt%) and stirred for 1 h. The mixture was dropped into a solution with $CaCl_2$ (3 wt%) and glutaraldehyde (1 wt%) at 95 °C using a syringe pump to obtain EWP/SPI hydrogel beads [33–35]. To remove superfluous reagents, the beads were washed several times using deionized water. Finally, EWP/SPI hydrogel beads were desiccated using

freeze-drying technology. The synthetic process of EWP/SPI hydrogel beads is exhibited in Figure 1.

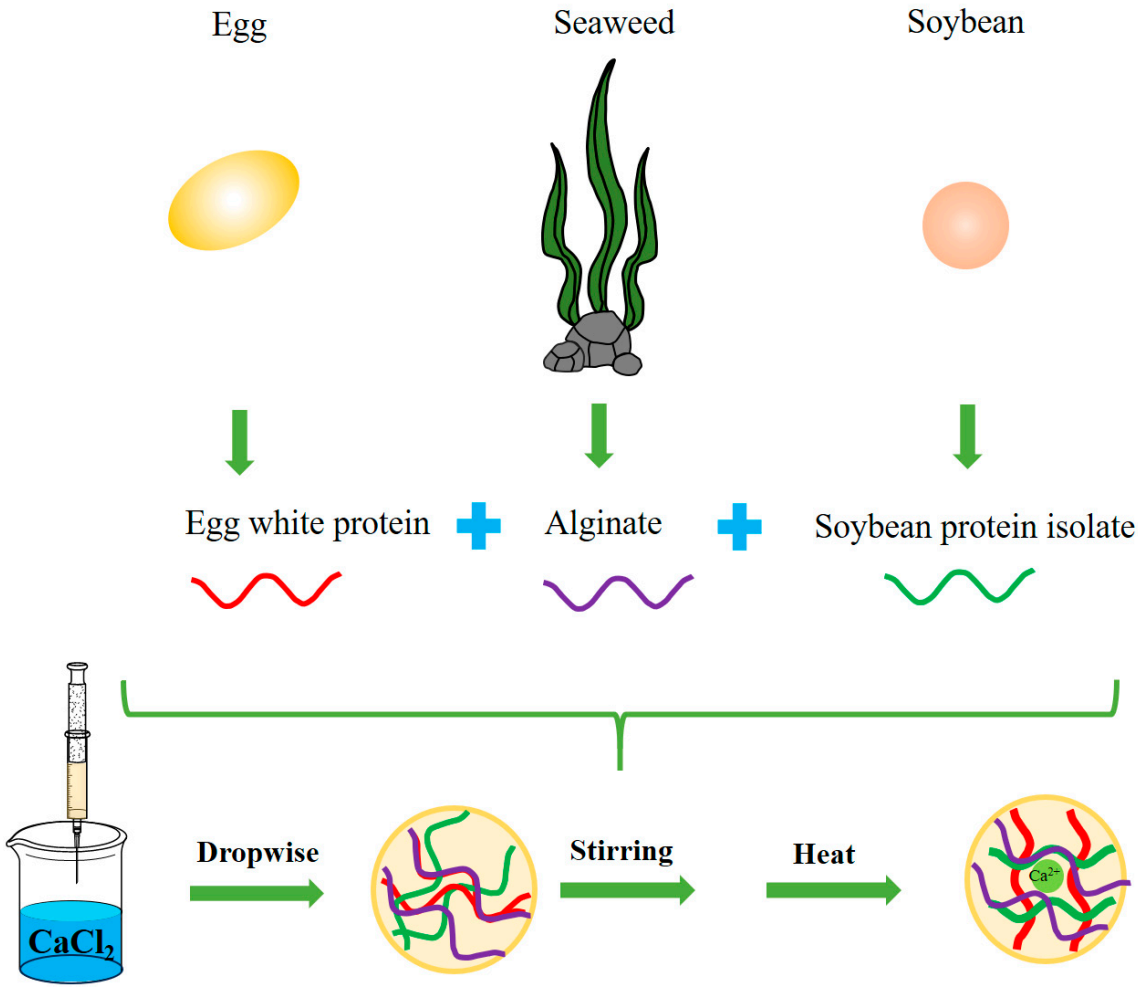

Figure 1. Schematic illustration of the preparation process of EWP/SPI hydrogel beads.

2.3. Characterisations

The morphology and chemical compositions of the as-fabricated beads were characterized by scanning electron microscope (SEM) with energy-dispersive spectrometry (EDS). The functional groups were analyzed by Fourier transform infrared spectroscopy (FTIR). The specific surface area within the relative pressure range (P/P_0) was calculated by surface area using Brunauer–Emmett–Teller (BET) and Barrett–Joyner–Halenda (BJH) methods. The concentrations of MB in the solution were measured by UV–Vis spectrometer (UV–Vis). The thermal stability of the beads was measured with a thermogravimetric analyzer (TGA) from 30 to 600 °C under a nitrogen atmosphere. The static contact angle was measured using a contact angle meter at the room temperature.

2.4. Adsorption Experiments

2.4.1. Adsorption of MB

In total, 10 mg EWP and EWP/SPI hydrogel beads were added into a 50 mL conical flask including 20 mL dye aqueous solution (50 $mg \cdot L^{-1}$) with a pH value of 7. The flask was stirred at 25 °C for 60 min. Then, 1 mL solution was taken out and diluted before UV–Vis spectrometry measurement.

2.4.2. Optimization of the Performance of EWP/SPI Hydrogel Beads

To optimize the adsorption performance of EWP/SPI hydrogel beads, influence of adsorption dose, pH, and adsorption time were investigated at 25 °C. Briefly, 5–25 mg beads were added to 20 mL MB solution with a concentration from 50 to 300 mg·L^{-1} (pH from 4 to 10) for 480 min in a shaking incubator at 200 rpm. After adsorption completion, the adsorption performance of the beads was characterized by the comparison of the residual MB concentration with the initial concentration using a UV–Vis spectrophotometer. The equilibrium adsorption capacity (q_e, mg·g^{-1}), adsorption capacity at time t (q_t, mg·g^{-1}), and removal rate (%) were calculated using the following formulas [31]:

$$q_e = \frac{C_0 - C_e}{m} \times V \quad (1)$$

$$q_t = \frac{C_0 - C_t}{m} \times V \quad (2)$$

$$\text{Removal rate} = \frac{C_0 - C_t}{C_0} \times 100 \quad (3)$$

where C_0 (mg·L^{-1}) is the initial contaminant concentration, C_e (mg·L^{-1}) is the MB concentration at the equilibrium, C_t (mg·L^{-1}) is the MB concentration at time t, V (L) is the volume of the MB solution, and m is the weight of the EWP/SPI hydrogel beads (g).

2.5. Stability of EWP/SPI Hydrogel Beads

2.5.1. Wettability of EWP/SPI Hydrogel Beads

To check the floatability of EWP/SPI hydrogel beads, we firstly evaluated the wettability of beads via measuring the water contact angle (WCA). Briefly, 10 µL deionized water was dropped onto the surface of the EWP/SPI hydrogel and then the WCA was measured using a contact angle meter. Note that at least five locations on the hydrogel were gauged to estimate the average WCA.

2.5.2. Floatability of EWP/SPI Hydrogel Beads

A total of 25 pieces of EWP/SPI hydrogel beads were immersed in 50 mL water with MB for 7 days, and we recorded the number of floating EWP/SPI beads. Floating rate (%) was determined by Equation (4).

$$\text{Floating rate} = \frac{F_t}{25} \times 100 \quad (4)$$

where F_t and 25 are the number of hydrogel beads floating at time t and the initial number of hydrogel beads.

2.6. Recyclability Experiments

The regeneration performance of the beads was determined by five adsorption–desorption cycles. In each cycle, 10 mg EWP/SPI beads were added into a 50 mL conical flask including MB solution (100 mg·L^{-1}, 20 mL, pH 7) under 120 rpm in a shaker. After an equilibration for 12 h, EWP/SPI beads absorbed with MB were immersed in 1 mol/L HCl for desorbing. After a desorption for 24 h, the beads were filtrated, washed, dried, and reused in the next adsorption cycle.

3. Results and Discussion

3.1. Characterization of EWP/SPI Hydrogel Beads

To analyze adsorption performance of EWP/SPI hydrogel beads, the morphological structures were precisely investigated. As shown in Figure 2a, the surface of pure EWP hydrogel composing of massive lamella exhibited some crosslinking points. The diameters of the EWP hydrogel ranged from 13 to 18 µm (Figure 2c). As a comparison, the surface of EWP/SPI hydrogel beads exhibited an apparent 3D network structure with massive

crosslinking points (Figure 2b). The range of pore diameter was from 0.32 to 3.02 µm, which is much smaller than those of EWP, as shown in Figure 2d, indicating that the addition of SPI into the EWP hydrogel decreases the pore diameter and increases the porosity the hydrogel. Based on the above results, the porous network structure may be due to the synergistic effect of the gelling of EWP and SPI, hydrogen bond interaction between EWP and SPI, and the complexation reaction with Ca^{2+} facilitating the crosslink of EWP, SPI with SA, leading to the formation of more porous structures.

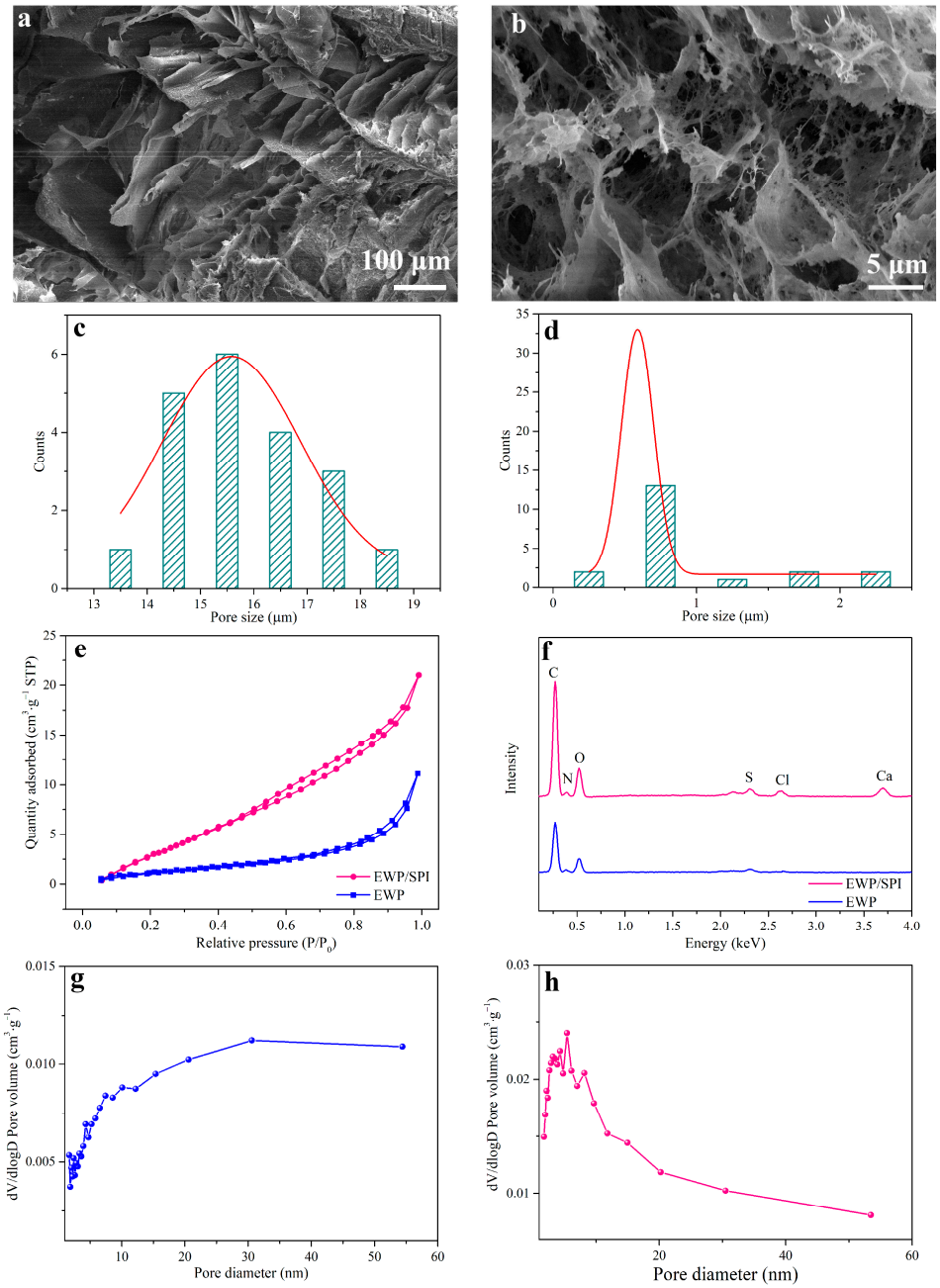

Figure 2. The morphology analysis of the as-fabricated EWP and EWP/SPI hydrogel beads. (**a**) SEM image of EWP hydrogel, (**b**) SEM images of EWP/SPI hydrogel beads, (**c**) pore size distribution histogram of EWP hydrogel, (**d**) pore size distribution histogram of EWP/SPI hydrogel beads, (**e**) N_2 adsorption–desorption isotherms of EWP and EWP/SPI hydrogel beads, (**f**) EDS of EWP and EWP/SPI hydrogel beads, (**g**) pore size distribution of EWP, and (**h**) pore size distribution of EWP/SPI hydrogel beads.

The N_2 adsorption/desorption isotherms of EWP and EWP/SPI hydrogel beads are presented in Figure 2e. The specific surface area of EWP/SPI (26.55 $m^2 \cdot g^{-1}$) increased by ~3 times more than EWP (6.50 $m^2 \cdot g^{-1}$). Such increases are consistent with a decrease in mean pore diameter from about 10.89 of EWP (Figure 2g) to 4.89 nm of EWP/SPI (Figure 2h), indicating the primarily mesopore structure in EWP and EWP/SPT hydrogel. The obtained isotherm conforms to typical Langmuir IV type, indicating a mesoporous structure in the beads as well. The N_2 adsorption/desorption amount of EWP/SPI is obviously higher than that of EWP at both low and high pressure. When $p/p_0 > 0.5$, the adsorption capacity increases sharply, and the desorption curve separates from the adsorption curve, exhibiting an H1 hysteresis loop [36]. This confirms that the hydrogel beads are chiefly composed of mesoporous structures, with capillary condensation of N_2 to fill the mesopores occurred in the adsorption process. Hence, mesopores are favorable for the adsorption of MB molecule via mesopore-filling mechanism.

To investigate the adsorption performance of the EWP/SPI hydrogel beads, EDS was employed to verify the elemental composition of the beads. As shown in Figure 2f, the elements C, O, N, S, Ca, and Cl can be identified in the spectrometry (red curve). C, O, and N are the most common elements of EWP and SPI. The calcium element originates from calcium alginate due to the reaction between sodium alginate and $CaCl_2$. As a comparison, pure EWP is just composed of C, O, N, and S (blue curve).

To further investigate the adsorption performance of the EWP/SPI hydrogel beads, the functional groups of the beads were characterized using FTIR spectroscopy, as shown in Figure 3a. A broadband peak between 3100 and 3700 cm^{-1} corresponds to −OH stretching vibration of EWP (in blue curve). A peak at 2960 cm^{-1} is attributable to stretching vibration of −CH. The peaks at 1650 and 1530 cm^{-1} are derived from the vibration of C=O and −NH, respectively. The peaks at 1363 and 1070 cm^{-1} belong to the vibration of C−O and C−O−C. As a comparison, the peaks in the red curve at 1644, 1538, 1420, and 1030 cm^{-1} belong to C=O stretching (amide I), N−H bending (amide II), C−N stretching (amide III), and C−C, confirming the successful formation of EWP/SPI hydrogel beads.

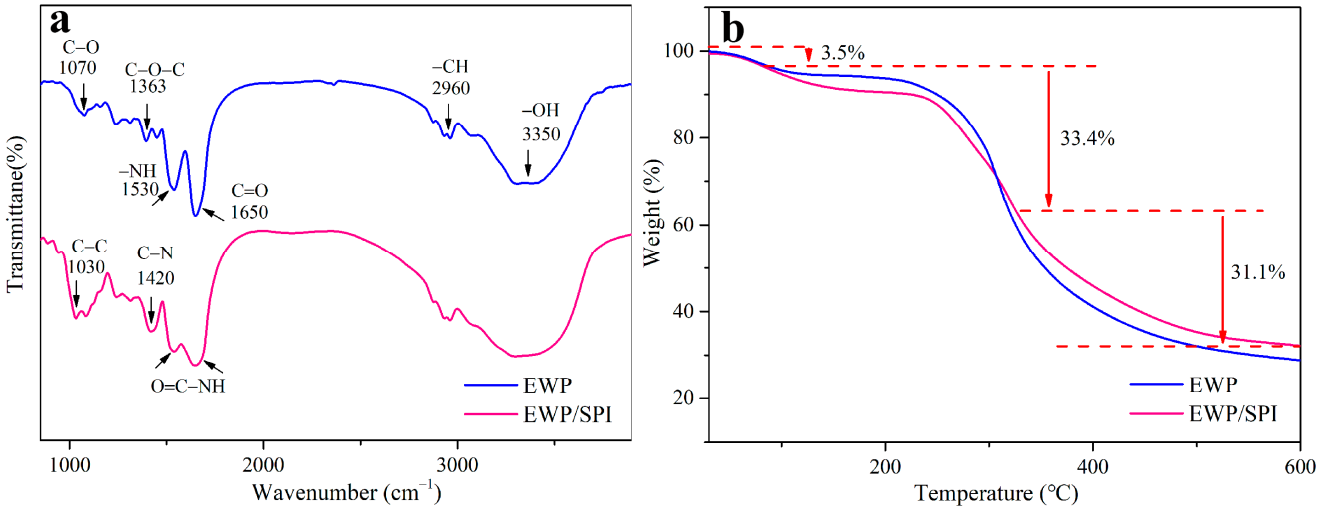

Figure 3. Chemical composition analysis of as-synthesized EWP/SPI hydrogel beads. (**a**) FTIR spectra of EWP and EWP/SPI hydrogel beads. (**b**) TGA analysis of EWP and EWP/SPI hydrogel beads.

TGA was used to characterize the thermal stability of the EWP/SPI hydrogel beads. As shown in Figure 3b, the TGA curves of EWP/SPI show a significant amount of weight loss, of about 3.5%, due to dehydration before 85 °C. Between 85 and 321 °C, EWP/SPI hydrogel beads exhibit an obvious mass loss of 33.4% due to the initial decomposition and dehydroxylation of organic components as well as the destruction of hydrogen bonds [29]. In the last stage (321−600 °C), a mass loss of 31.1% from EWP/SPI hydrogel beads is caused by the further decomposition and carbonization of organic components in EWP/SPI

hydrogel beads. Comparison with the residue of EWP/SPI (32%), the residue content of EWP hydrogel is lower (28.9%). These obtained results declare a higher thermal stability of EWP/SPI hydrogel beads, probably attributed to the formation of hydrogen bonds between EWP, SPI, and SA.

3.2. Adsorption Performance of EWP/SPI Hydrogel Beads

Figure 4 shows the UV–Vis spectra of MB in contact with EWP, EWP/SPI hydrogel beads. The UV–Vis absorption peak at 665 nm was used to monitor the changes in concentration before and after the treatment of various hydrogels. The UV–Vis absorption spectra of MB treatment with EWP and EWP/SPI hydrogel beads for 60 min are shown in Figure 4. The absorbance of MB treated with EWP/SPI is lower than that treated with EWP, suggesting that EWP/SPI hydrogel beads adsorb much more MB compared with EWP hydrogel. This result indicates that the EWP/SPI hydrogel beads can enhance the adsorption capacity of the hydrogel compared with pure EWP hydrogel through the synergistic effect between EWP, SPI, and SA.

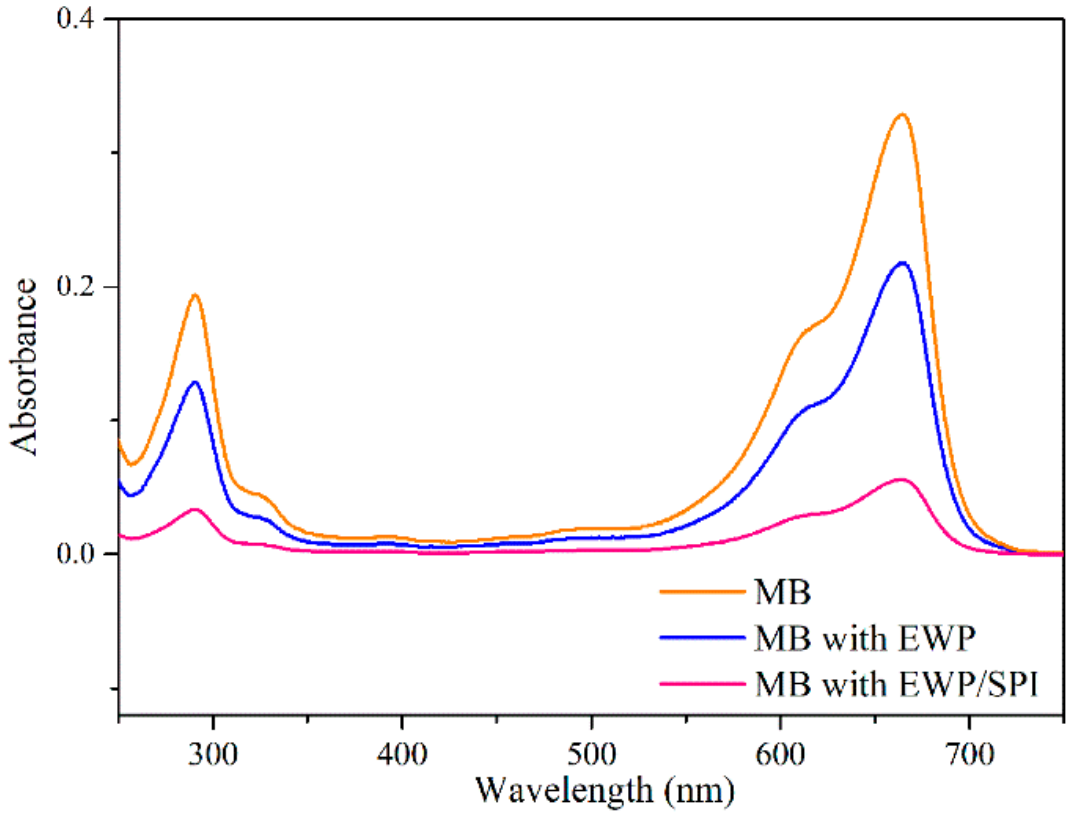

Figure 4. The UV–Vis spectra of MB treated with different hydrogels for 60 min.

To maximize the adsorption capacity of the prepared beads, we investigated the influence of adsorption parameters (adsorbent dosage, pH, and time) in the adsorption process. The effects of absorbent dosage on adsorption capacity and percentage contaminant removal were analyzed by adding 5–25 mg EWP/SPI beads into 100 mg·L^{-1} MB solution with a volume of 20 mL. As shown in Figure 5a, with the increase in the amount of the adsorbent, the removal rate increased from 75 to 99% due to the increase in the adsorption sites and surface area. However, with the increase in the dose of the adsorbent, q_e decreased from 300 to 79.2 mg·g^{-1}. The decrease in q_e arose mainly due to the lower utilization of active sites employed to adsorb MB molecules on the adsorbent surface.

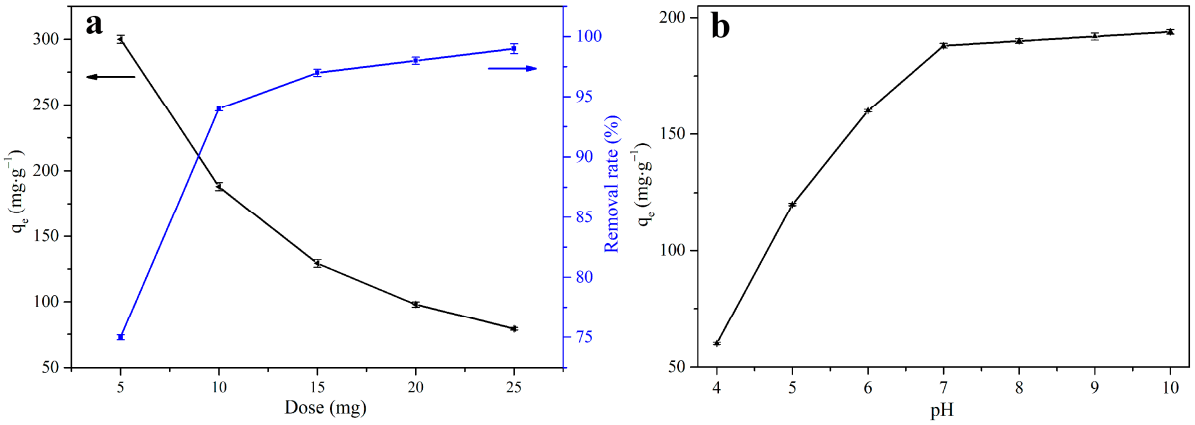

Figure 5. Effects of (**a**) adsorbent dosage and (**b**) pH on the adsorption of MB on EWP/SPI hydrogel beads.

To evaluate the influence of pH in the solution, the adsorption capacity of the EWP/SPI beads was investigated across a pH range of 4 to 10, shown in Figure 5b. When the pH increased from 4 to 10, the MB adsorption capacity increased from 60 to 194 mg·g^{-1}. The low adsorption capacity in acidic condition is attributed to positively charged H^+ occupying the adsorption sites and competing with cationic dyes in the adsorption process. With an increase in solution pH, the carboxyl group and hydroxyl group of EWP/SPI beads were deprotonated and enhanced the interactions with the MB cation. Therefore, weakly basic solutions were chosen for further measurements.

To evaluate the adsorption efficiency of EWP/SPI hydrogel beads in the adsorption process, we investigated the relation of adsorption capacity to contact time. As shown in Figure 6, the adsorption capacity of EWP/SPI hydrogel beads MB sharply increased to 180.0 mg·g^{-1} within 60 min and eventually reached an equilibrium concentration of 188.7 mg·g^{-1} at approximately 480 min at 25 °C with a pH value of 7. At the beginning of the adsorption, the fast adsorption rate was owing to abundant adsorption sites on EWP/SPI hydrogel beads, resulting from the porous structure and the massive functional groups on the surface of the hydrogel. This boosted intraparticle diffusion and efficient adsorption of the MB molecule. Subsequently, after 60 min, the adsorption rate lowered due to a decrease in available active sites on the EWP/SPI hydrogel beads, leading to a dynamic adsorption–desorption process in the beads.

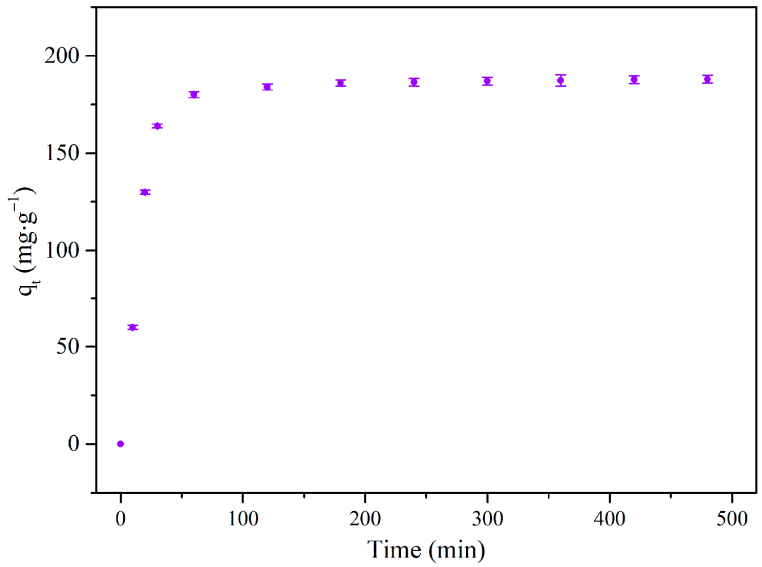

Figure 6. Effect of time on the adsorption of MB on EWP/SPI hydrogel beads.

3.3. Adsorption Kinetics of EWP/SPI Hydrogel Beads

To better understand the adsorption process, adsorption kinetics was used to analyze the adsorption reaction of EWP/SPI hydrogel beads. The adsorption process was studied using a pseudo-first-order kinetic model, a pseudo-second-order kinetic model, the Elovich kinetic model, and the intraparticle diffusion model. The pseudo-first-order model (Equation (5)), pseudo-second-order model (Equation (6)), Elovich kinetic model (Equation (7)), and intraparticle diffusion model (Equation (8)) are formulated as follows [31]:

$$q_t = q_e\left(1 - e^{-k_1 t}\right) \tag{5}$$

$$q_t = \frac{q_e^2 k_2 t}{1 + k_2 q_e t} \tag{6}$$

$$q_t = \frac{\ln(\alpha\beta)}{\beta} + \frac{\ln(t)}{\beta} \tag{7}$$

$$q_t = k_i t^{1/2} + c_i \tag{8}$$

where q_t and q_e in the equilibrium are the adsorption capacity at time t and equilibrium adsorption capacity. k_1 (min^{-1}) and k_2 ($g{\cdot}mg^{-1}{\cdot}min^{-1}$) are the rate constant of the pseudo-first-order model and the pseudo-second-order model. α ($mg{\cdot}g^{-1}{\cdot}min^{-1}$) denotes the initial adsorption rates, β ($g{\cdot}mg^{-1}$) refers to the parameters related to chemisorption activation energy and surface coverage extent. k_i ($mg{\cdot}g^{-1}{\cdot}min^{-1/2}$) is the rate constant of the intraparticle diffusion model and c_i ($mg\ mg^{-1}{\cdot}g$) is a constant associated with the thickness of the boundary layer.

As seen in Figure 7a, the pseudo-first-order model, pseudo-second-order model, and Elovich kinetic model were simulated by nonlinear regression analysis. The kinetic parameters and correlation coefficients are summarized in Table 1. Compared with the pseudo-second-order model (R^2 = 0.953) and Elovich kinetic model (R^2 = 0.875), the pseudo-first-order model (R^2 = 0.985) is more consistent, with the kinetic adsorption data describing the adsorption process. To further explore the interaction of the EWP/SPI beads and MB, all data were fitted by the intraparticle diffusion model. As shown in Figure 7b, the fitting line is nonlinear and can be divided into two parts with different slopes. The first stage (R^2 = 0.908), with a slope of 19.561, is a rapid adsorption stage due to transportation of the MB from the solution to the surface of the EWP/SPI beads in this process. In the second stage, the slope of the fitting line (R^2 = 0.904) is reduced to 0.337, which implies that the adsorption process is much slower than the first stage. This stage is dominated by the reaction between the EWP/SPI beads and the MB.

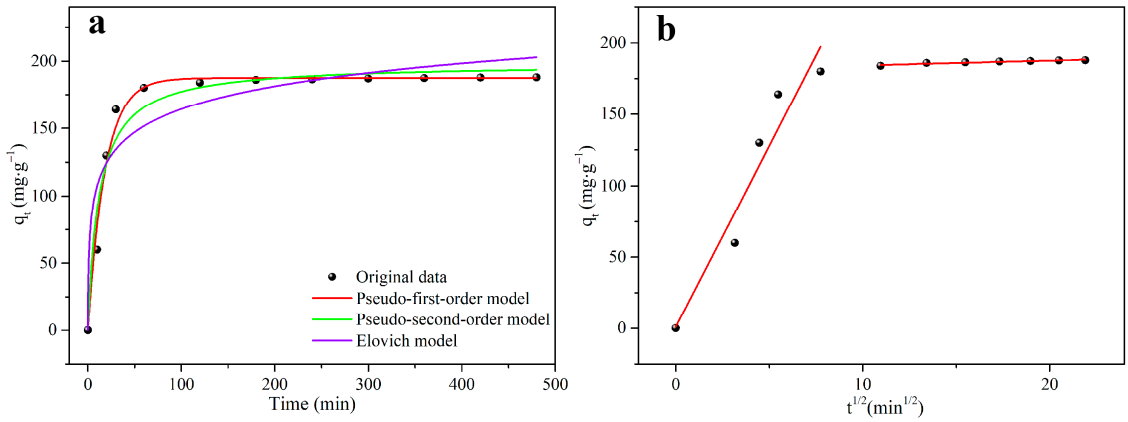

Figure 7. Model fitting of the adsorption of EWP/SPI hydrogel beads for MB. (**a**) Adsorption kinetics. (**b**) Intraparticle diffusion model.

Table 1. Kinetics parameters of MB adsorption on EWP/SPI hydrogel beads.

Kinetic Model	Parameter	Values
Pseudo-first-order kinetic model	k_1 (min^{-1})	0.0546
	q_e ($mg{\cdot}g^{-1}$)	187.495
	R^2	0.985
Pseudo-second-order kinetic model	$k_2 \times 10^4$ ($g{\cdot}mg^{-1}{\cdot}g^{-1}$)	4.212
	q_e ($mg{\cdot}g^{-1}$)	198.417
	R^2	0.95293
Elovich kinetic model	α ($mg{\cdot}g^{-1}{\cdot}min^{-1}$)	190.590
	β ($g{\cdot}mg^{-1}$)	0.04051
	R^2	0.875
Intraparticle diffusion model	$k_{i,1}$ ($mg{\cdot}g^{-1}{\cdot}min^{-1/2}$)	19.561
	$c_{i,1}$ ($mg{\cdot}g^{-1}$)	1.0883
	R^2	0.908
	$k_{i,2}$ ($mg{\cdot}g^{-1}{\cdot}min^{-1/2}$)	0.337
	$c_{i,2}$ ($mg{\cdot}g^{-1}$)	180.952
	R^2	0.904

3.4. Adsorption Isotherm of EWP/SPI Hydrogel Beads

To further explain the interaction between solid EWP/SPI beads and MB molecule in solution, the adsorption isotherm models (Langmuir (Equation (9)), Freundlich (Equation (10)), and Temkin (Equation (11)) were used to perform nonlinear fitting to these experimental data and explore the adsorption equilibrium in the adsorption process. The Langmuir model assumes monolayer formation at specific homogeneous sites within the adsorbent, while the Freundlich model refers to the heterogeneity of adsorption sites and multilayer adsorption [37]. Finally, the Temkin model considers indirect interactions between adsorbent and adsorbate molecules.

The expressions of the adsorption isotherm models are presented below [31,36].

$$q_e = \frac{q_m K_L C_e}{1 + K_L c_e} \tag{9}$$

$$q_e = K_f C_e^{1/n} \tag{10}$$

$$q_e = B_T \ln(A_T C_e) \tag{11}$$

Here, K_L ($L{\cdot}g^{-1}$) and K_f ($mg^{1-1/n}{\cdot}L^{1/n}{\cdot}g^{-1}$) represent the absorption constants of the Langmuir model, the Freundlich model, and the Temkin model, respectively. B_T ($J{\cdot}mol^{-1}$) is the energy constant in the Temkin isotherm model. C_e is the concentration of MB at equilibrium. A_T describes ($L{\cdot}mg^{-1}$) the equilibrium binding constant. n represents the degree of irregularity of the adsorbent surface.

The equilibrium adsorption relationships between MB molecule and EWP/SPI hydrogel beads are explained using the adsorption isotherm. The adsorption isotherm models are fitted using the nonlinear regression technique to avoid some errors in linearization. The parameters of the adsorption isotherms are listed in Table 2. As shown in Figure 8, all the isotherm models had a good correlation with the experimental data. The correlation coefficient (R^2) of the isotherm models ranged from 0.910 to 0.989. Among the three isotherm models, the adsorption process expressed a greater consistency with the Langmuir model (R^2 = 0.989) compared with the other two models, indicating monolayer adsorption on EWP/SPI hydrogel beads with effective adsorption ability at each adsorption point. According to the fitting results, the adsorption of MB on the EWP/SPI beads was conducted through reaction with oxygen-containing functional groups. The value of the separation factor (R_L) was calculated to be 0.052, indicating spontaneous and favorable adsorption. The maximum adsorption capacity of the EWP/SPI beads calculated by the Langmuir model was 336.265 $mg{\cdot}g^{-1}$.

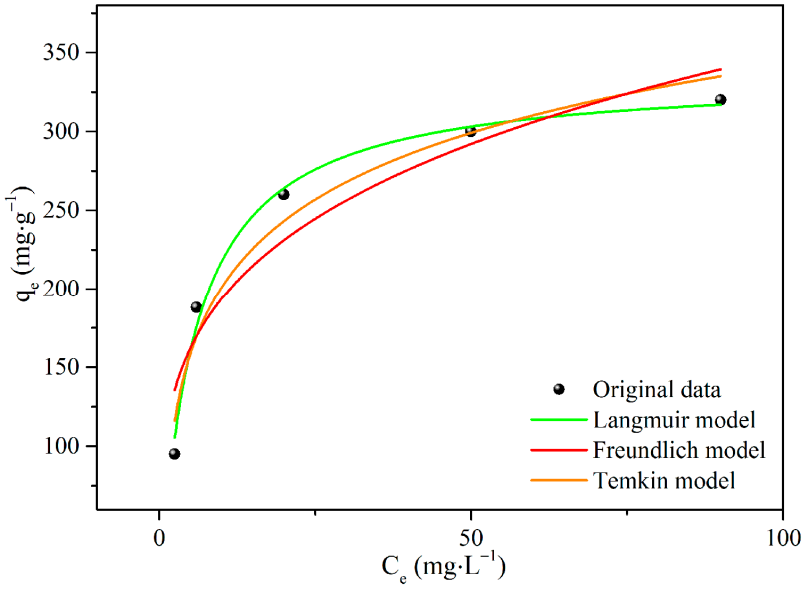

Figure 8. Adsorption isotherm fitting of the adsorption of EWP/SPI hydrogel beads for MB.

Table 2. Isotherm parameters of MB adsorption on EWP/SPI hydrogel beads.

Isotherm Models	Parameter	Values
Langmuir	q_m (mg·g^{-1})	336.265
	K_L (L·mg^{-1})	0.183
	R^2	0.989
Freundlich	K_f (mg$^{1-1/n}$·L$^{1/n}$·g^1)	107.353
	n	3.909
	R^2	0.910
Temkin	B_T (J·mol^{-1})	61.083
	A_T (L·mg^{-1})	2.677
	R^2	0.949

3.5. Thermodynamic Studies of EWP/SPI Hydrogel Beads

To further analyze the adsorption mechanisms of MB on the EWP/SPI beads, the change in thermodynamic adsorption parameters (Gibbs free energy (*G*), entropy (*S*), and enthalpy (*H*)) were calculated the following mathematical expressions [31,36]:

$$\Delta G = \Delta H - T\Delta S \tag{12}$$

$$\ln\left(\frac{q_e}{C_e}\right) = -\frac{\Delta H}{RT} + \frac{\Delta S}{R} \tag{13}$$

In the expression, T (K) is absolute temperature in Kelvin, and R (8.314 J·mol^{-1}·K^{-1}) is the universal gas constant. The values of ΔH and ΔS can be calculated from the linear fit of expressions (14) using $\ln(q_e/c_e)$ versus $1/T$. The thermodynamic parameters of MB adsorption are estimated using the Van't Hoff equation (Equation (13)). The calculated results of ΔH, ΔS, and ΔG values are -40.085 kJ·mol^{-1}, -105.955 J·mol^{-1}·K^{-1}, and -8.511 kJ·mol^{-1}. The value of ΔG is negative ($\Delta G < 0$) and between -20 to 0 kJ/mol at experimental temperatures, which indicates that this adsorption process occurred spontaneously and physisorption predominated the adsorption of MB. Moreover, the absolute value of increases with decrease in temperature suggests that the physisorption predominated adsorption and lower temperatures are conducive to the adsorption of MB [38]. The value of ΔH is also negative, which implies that the adsorption process is exothermic.

The negative value of entropy changes shows that the adsorption reduces disorder at the solid–solute interface.

To further understand adsorption mechanism, the Dubinin–Radushkevich (D–R) isotherm model was employed to describe adsorption on both heterogeneous and homogenous surfaces. The D–R model is expressed as follows:

$$\ln q_e = lnq_m - B\varepsilon^2 \tag{14}$$

Here, B represents a constant related to the mean free energy of adsorption ($mol^2 \cdot kJ^{-2}$), q_m refers the theoretical saturation capacity, and ε represents the Polanyi potential, which is calculated as follows:

$$\varepsilon = RT\ln\left(1 + \frac{1}{C}\right) \tag{15}$$

T (K) refers to the absolute temperature, and R (J $mol^{-1} \cdot K^{-1}$) indicates the gas constant. The mean energy of adsorption (E) can be estimated using the following expression:

$$E = \frac{1}{\sqrt{-2B}} \tag{16}$$

According to Equations (14)–(16), E is calculated as 2.017 $kJ \cdot mol^{-1}$, which is below 5 $kJ \cdot mol^{-1}$, providing important information regarding adsorption mechanism. Note that the value of E ranges from 1 to 8 $kJ \cdot mol^{-1}$, 8 to 16 $kJ \cdot mol^{-1}$, and 20 to 40 $kJ \cdot mol^{-1}$, where the adsorption process corresponds to physical adsorption, ion exchange, and chemisorption, respectively. E is calculated as 2.017 $kJ \cdot mol^{-1}$, which is below 5 $kJ \cdot mol^{-1}$, validating that the physical adsorption dominates the adsorption process of EWP/SPI towards MB.

3.6. Floatability Performance of EWP/SPI Hydrogel Beads

EWP/SPI hydrogel beads are completely hydrophilic as the WCA is ~0°and absorbed water droplets immediately when the water droplet is placed on the surface of the hydrogel (inset of Figure 9). The floatability of hydrogel beads is favorable for MB absorption and separation after the adsorption process [33]. Figure 9 shows the floating performance of EWP/SPI hydrogel beads in water over 7 days. The floatation rates of beads are 100% for the first two days, followed by a decrease with the increase in immersion time. Even after soaking for 7 days, the floating rates of all beads are still higher than 80%. These results imply that the EWP/SPI hydrogel beads provide great potential for reuse during practical applications.

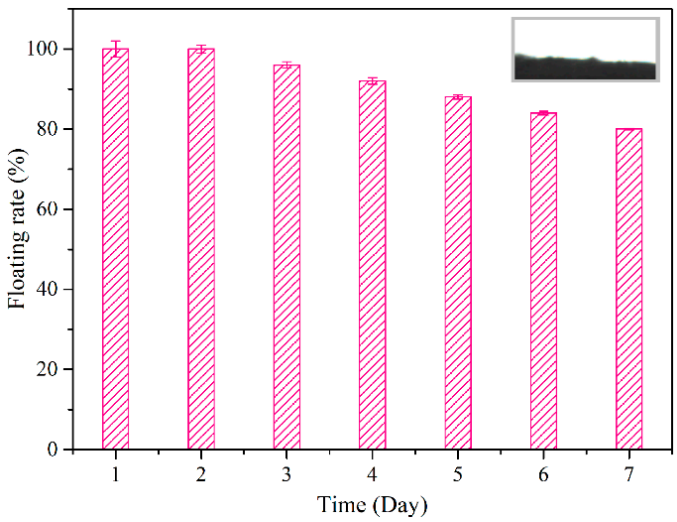

Figure 9. The floating behavior of EWP/SPI hydrogel beads in water for 7 days (the inset is WCA of EWP/SPI).

3.7. Regeneration Performance of EWP/SPI Hydrogel Beads

To evaluate the regeneration performance of EWP/SPI hydrogel beads, a repetitious adsorption–desorption of MB was performed for five cycles, where 10 mg EWP/SPI beads were added to the MB solution with a concentration of 100 mg·mL^{-1}. After an adsorption of 12 h, EWP/SPI beads with MB were filtered and immersed in 1 mol·L^{-1} HCl to desorb the absorbed MB. Under strongly acidic condition, the interaction between MB and EWP/SPI hydrogel beads was electrostatic repulsion. The H^+ derived from HCl interacted with the adsorptive site EWP/SPI hydrogel beads more strongly, leading to the desorption of MB. After a careful collection and cleaning, the beads were employed for repeated absorption. Then the adsorption capacities were calculated and compared with the initial value. The adsorption capacity and adsorption efficiency of EWP/SPI hydrogel beads is shown in Figure 10. After five adsorption–desorption cycles, the adsorption efficiency of EWP/SPI beads decreased to 82%. Thus, the EWP/SPI beads are adsorbent with preferable reusability.

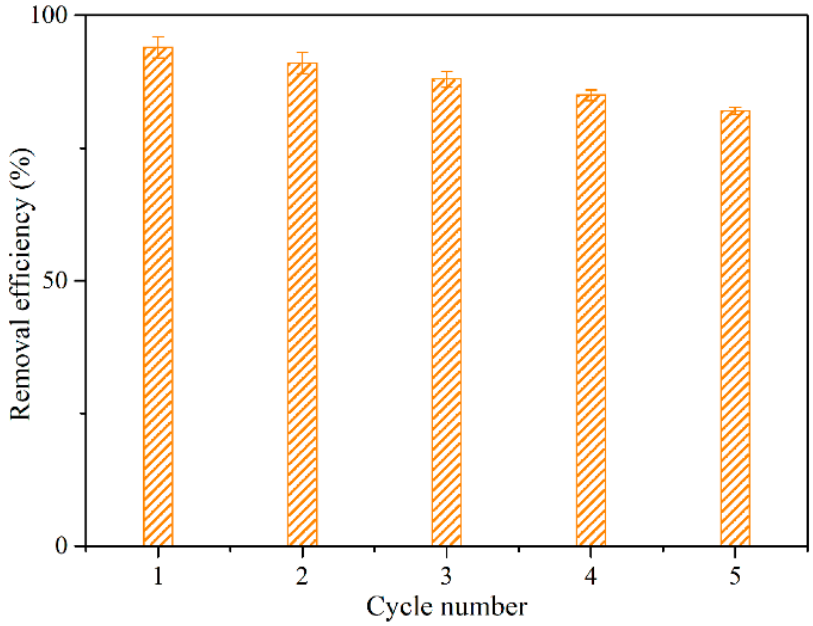

Figure 10. Regeneration performance of EWP/SPI hydrogel beads towards the adsorption of MB.

FTIR spectra of EWP/SPI adsorbing MB (the first cycle) and EWP/SPI (after desorption of MB) were performed to gain more adsorption mechanisms in Figure 11. Compared with EWP/SPI hydrogel beads, a new absorption band at 3420 cm^{-1} in the blue curve of MB adsorbed EWP/SPI, indicating an overlapping peak from −OH stretching vibration and -NH in the MB molecule. A decrease in peak intensity at 3420 cm^{-1} of −OH and −NH indicates a hydrogen bonding interaction between −NH and −OH. Furthermore, a decrease in peak intensity at 1650 (C=O), 1030 cm^{-1} (C−O), and a shift from 1650 to 1640 cm^{-1} indicates the successful adsorption of MB molecules on EWP/SPI hydrogel beads. After a desorption of MB from EWP/SPI using HCl, the disappearance of characteristic absorption peak at 3420 cm^{-1} (-NH), and increase in peak intensity at 1650 (C=O) and 1030 cm^{-1} (C−O), confirm the successful desorption of MB from EWP/SPI hydrogel beads.

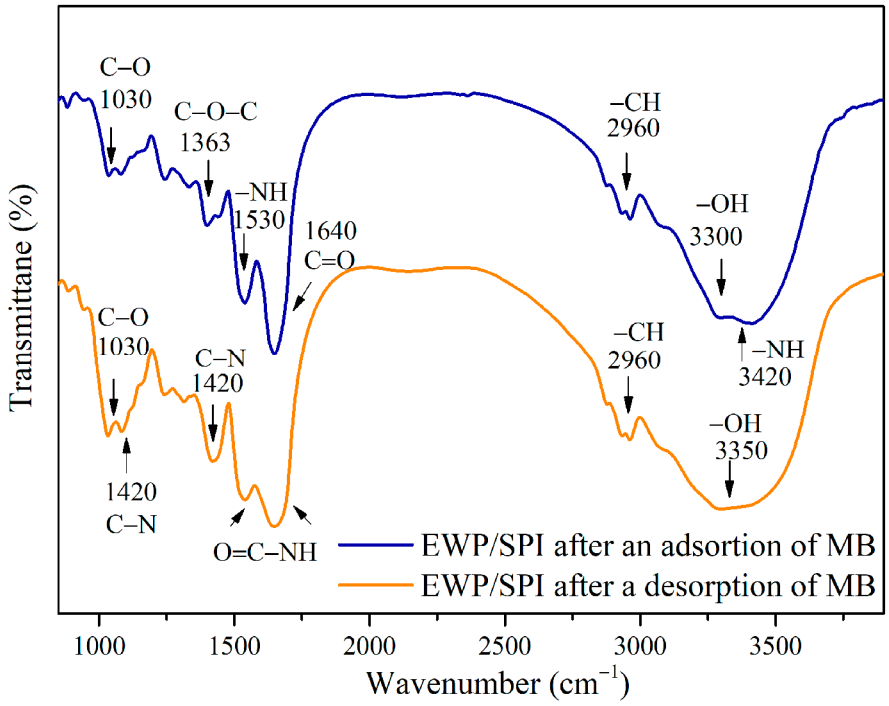

Figure 11. FTIR spectra of EWP/SPI hydrogel beads before and after desorption of MB.

3.8. Comparison of Adsorption Performance of EWP/SPI Hydrogel Beads with Other Adsorbents

EWP/SPI beads showed a relatively high adsorption capacity for MB. Based on the Langmuir model, the maximum adsorption capacity of EWP/SPI hydrogel beads for MB was 336.265 mg g^{-1}. A comparison of adsorption capacity with other reported adsorbents is listed in Table 3. The adsorption capacity of EWP/SPI hydrogel beads was larger than that of EWP/graphene oxide (91.7 mg·g^{-1}) and superabsorbent polymer-activated charcoal (213.2 mg·g^{-1}), and much higher than that of polyvinyl alcohol-alginate/bentonite (51.34 mg·g^{-1}) and modified soybean straw activated carbon (41.96 mg·g^{-1}). These data declare that the synthesized EWP/SPI hydrogel beads can be employed as an adsorbent for MB.

Table 3. Comparison of maximum adsorption of EWP/SPI hydrogel beads with various adsorbents.

Type of Adsorbent	q_m (mg·g^{-1})	References
EWP/graphene oxide	91.7	[24]
Polyvinyl alcohol-alginate/bentonite	51.34	[39]
Modified soybean straw activated carbon	41.96	[40]
Superabsorbent polymer-activated charcoal	213.2	[41]
EWP/SPI hydrogel	336.265	This work

4. Conclusions

In this paper, low-cost and efficient EWP/SPI hydrogel beads reinforced with calcium alginate were successfully synthesized by a one-step simple chemical crosslinking. Here, the crosslinking of SPI formed a first-order network, and then the crosslinking of EWP component formed a second-order network. The addition of alginate into hydrogels acted as a framework and mechanical property reinforcement agent to form a third-order network and enhance the mechanical property of hydrogels through crosslinking with Ca^{2+}. The as-prepared EWP/SPI hydrogel beads exhibited a distinctive 3D porous structure with excellent structural stability and floatability. The maximum adsorption capacity of

EWP/SPI hydrogel beads towards MB was 336.265 $mg \cdot g^{-1}$. Moreover, the prepared hydrogel beads exhibited obvious reusability after five cycles of adsorption–desorption. These results indicate that the EWP/SPI hydrogel beads show a favorable adsorption performance in water treatment. We envision that as-prepared beads offer a possibility for generating multifunctional beads applied in water disposal.

Author Contributions: Investigation, methodology, validation, and writing: X.W. and M.Z. All authors have read and agreed to the published version of the manuscript.

Funding: This work was financially funded by the Natural Science Foundation of Jiangsu Province (grant number BK20201060), the funding for school-level research projects of Yancheng Institute of Technology (grant number xjr2020003).

Data Availability Statement: The original contributions presented in the study are included in the article; further inquiries can be directed to the corresponding author.

Conflicts of Interest: The authors declare no conflicts of interest.

References

1. Wang, M.; Janssen, A.B.G.; Bazin, J.; Strokal, M.; Ma, L.; Kroeze, C. Accounting for interactions between Sustainable Development Goals is essential for water pollution control in China. *Nat. Commun.* **2022**, *13*, 730. [CrossRef] [PubMed]
2. Lin, L.; Yang, H.; Xu, X. Effects of water pollution on human health and disease heterogeneity: A review. *Front. Environ. Sci.* **2022**, *10*, 880246. [CrossRef]
3. Rahmatpour, A.; Alijani, N.; Alizadeh, A.H. Preparation of chitosan-based ternary nanocomposite hydrogel film by loading graphene oxide nanosheets as adsorbent for enhanced methylene blue dye removal. *Int. J. Biol. Macromol.* **2023**, *253*, 126585. [CrossRef] [PubMed]
4. Yagub, M.T.; Sen, T.K.; Afroze, S.; Ang, H.M. Dye and its removal from aqueous solution by adsorption: A review. *Adv. Colloid Interface Sci.* **2014**, *209*, 172–184. [CrossRef] [PubMed]
5. Xu, W.; Li, Y.; Wang, H.; Du, Q.; Li, M.; Sun, Y.; Cui, M.; Li, L. Study on the adsorption performance of casein/graphene oxide aerogel for methylene blue. *ACS Omega* **2021**, *6*, 29243–29253. [CrossRef]
6. Zeng, G.; He, Z.; Wan, T.; Wang, T.; Yang, Z.; Liu, Y.; Lin, Q.; Wang, Y.; Sengupta, A.; Pu, S. A self-cleaning photocatalytic composite membrane based on g-C_3N_4@MXene nanosheets for the removal of dyes and antibiotics from wastewater. *Sep. Purif. Technol.* **2022**, *292*, 121037. [CrossRef]
7. Wang, T.; Zheng, J.; Cai, J.; Liu, Q.; Zhang, X. Visible-light-driven photocatalytic degradation of dye and antibiotics by activated biochar composited with K^+ doped g-C_3N_4: Effects, mechanisms, actual wastewater treatment and disinfection. *Sci. Total Environ.* **2022**, *839*, 155955. [CrossRef]
8. Yin, Z.; Chen, X.; Zhou, T.; Xue, M.; Li, M.; Liu, K.; Zhou, D.P.; Ou, J.; Xie, Y.; Ren, Z.; et al. Mussel-inspired fabrication of superior superhydrophobic cellulose-based composite membrane for efficient oil emulsions separation, excellent anti-microbial property and simultaneous photocatalytic dye degradation. *Sep. Purif. Technol.* **2022**, *286*, 120504. [CrossRef]
9. Chen, L.; Hu, X.; Cai, T.; Yang, Y.; Zhao, R.; Liu, C.; Li, A.; Jiang, C. Degradation of Triclosan in soils by thermally activated persulfate under conditions representative of in situ chemical oxidation (ISCO). *Chem. Eng. J.* **2019**, *369*, 344–352. [CrossRef]
10. Atallah, C.; Mosadeghsedghi, S.; Kenari, S.L.D.; Hudder, M.; Morin, L.; Volchek, K.; Mortazavi, S.; Ben Salah, I. Removal of heavy metals from mine water using a hybrid electrocoagulation-ceramic membrane filtration process. *Desalin. Water Treat.* **2024**, *320*, 100730. [CrossRef]
11. Sefiddashti, F.T.; Homayoonfal, M. Nanostructure-manipulated filtration performance in nanocomposite membranes: A comprehensive investigation for water and wastewater treatment. *Heliyon* **2024**, *10*, e36874. [CrossRef] [PubMed]
12. Xiao, W.; Jiang, X.; Liu, X.; Zhou, W.; Garba, Z.N.; Lawan, I.; Wang, L.; Yuan, Z. Adsorption of organic dyes from wastewater by metal-doped porous carbon materials. *J. Clean. Prod.* **2021**, *284*, 124773. [CrossRef]
13. Xue, H.; Wang, X.; Xu, Q.; Dhaouadi, F.; Sellaoui, L.; Seliem, M.K.; Ben Lamine, A.; Belmabrouk, H.; Bajahzar, A.; Bonilla-Petriciolet, A.; et al. Adsorption of methylene blue from aqueous solution on activated carbons and composite prepared from an agricultural waste biomass: A comparative study by experimental and advanced modeling analysis. *Chem. Eng. J.* **2021**, *430*, 132801. [CrossRef]
14. Zhao, R.; Shi, X.; Ma, T.; Rong, H.; Wang, Z.; Cui, F.; Zhu, G.; Wang, C. Constructing mesoporous adsorption channels and MOF-polymer interfaces in electrospun composite fibers for effective removal of emerging organic contaminants. *ACS Appl. Mater. Interfaces* **2021**, *13*, 755–764. [CrossRef] [PubMed]
15. Yadav, S.; Asthana, A.; Singh, A.K.; Chakraborty, R.; Vidya, S.S.; Susan, M.A.B.H.; Carabineiro, S.A.C. Adsorption of cationic dyes, drugs and metal from aqueous solutions using a polymer composite of magnetic/β-cyclodextrin/activated charcoal/Na alginate: Isotherm, kinetics and regeneration studies. *J. Hazard. Mater.* **2021**, *409*, 124840. [CrossRef]

16. Dai, H.; Yuan, X.; Jiang, L.; Wang, H.; Zhang, J.; Zhang, J.; Xiong, T. Recent advances on ZIF-8 composites for adsorption and photocatalytic wastewater pollutant removal: Fabrication, applications and perspective. *Coord. Chem. Rev.* **2021**, *441*, 213985. [CrossRef]
17. Zhao, X.; Wang, X.; Lou, T. Preparation of fibrous chitosan/sodium alginate composite foams for the adsorption of cationic and anionic dyes. *J. Hazard. Mater.* **2021**, *403*, 124054. [CrossRef]
18. Kalidhasan, S.; Lim, Y.S.; Chu, E.A.; Choi, J.; Lee, H.Y. Phospholipid-derived Au and Au-Cu suspensions as efficient peroxide and borohydride activators for organic molecules degradation: Performance and sustainable catalytic mechanism. *Chemosphere* **2024**, *346*, 140567. [CrossRef]
19. Zhang, Z.; Tran, P.; Rumi, S.; Bergfeld, N.; Reid, T.W.; Abidi, N. Alginate/organo-selenium composite hydrogel beads: Dye adsorption and bacterial deactivation. *Int. J. Biol. Macromol.* **2024**, *280*, 135908. [CrossRef]
20. Yang, J.; Nie, J.; Bian, L.; Zhang, J.; Song, M.; Wang, F.; Lv, G.; Zeng, L.; Gu, X.; Xie, X.; et al. Clay minerals/sodium alginate/polyethylene hydrogel adsorbents control the selective adsorption and reduction of uranium: Experimental optimization and Monte Carlo simulation study. *J. Hazard. Mater.* **2024**, *468*, 133725. [CrossRef]
21. Zhang, T.; Chen, T.; Jiang, H.; Liu, J.; Wang, E.; Zhang, M.; Liu, X. pH-induced egg white protein foaming properties enhancement: Insight into protein structure and quantitative proteomic analysis at protein adsorption layer. *Food Hydrocoll.* **2023**, *144*, 109060. [CrossRef]
22. Chen, Y.S.; Ooi, C.W.; Show, P.L.; Hoe, B.C.; Chai, W.S.; Chiu, C.Y.; Wang, S.S.S.; Chang, Y.K. Removal of ionic dyes by nanofiber membrane functionalized with chitosan and egg white proteins: Membrane preparation and adsorption efficiency. *Membranes* **2022**, *12*, 63. [CrossRef] [PubMed]
23. Su, Y.; Wang, Y.; McClements, D.J.; Lu, C.; Chang, C.; Li, J.; Gu, L.; Yang, Y. Selective adsorption of egg white hydrolysates onto activated carbon: Establishment of physicochemical mechanisms for removing phenylalanine. *Food Chem.* **2021**, *364*, 130285. [CrossRef] [PubMed]
24. Jin, Y.; Du, Q.; Li, Y.; Zhang, Y.; Chen, B.; Wang, M.; Chen, K.; Sun, Y.; Zhao, S.; Jing, Z. Removal of methylene blue by crosslinked egg white protein/graphene oxide bionanocomposite aerogels. *Nanomaterials* **2022**, *12*, 2659. [CrossRef] [PubMed]
25. Farjami, T.; Babaei, J.; Nau, F.; Dupont, D.; Madadlou, A. Effects of thermal, non-thermal and emulsification processes on the gastrointestinal digestibility of egg white proteins. *Rends Food Sci. Technol.* **2021**, *107*, 45–56. [CrossRef]
26. Gharbi, N.; Labbafi, M. Effect of processing on aggregation mechanism of egg white proteins. *Food Chem.* **2018**, *252*, 126–133. [CrossRef]
27. Sun, S.; Xu, Y.; Maimaitiyiming, X. Egg white/gelatin/carboxymethylcellulose superbly bonded and biocompatible flexible self-adhesive multifunctional sensor. *Cellulose* **2024**, *31*, 6779–6795. [CrossRef]
28. Yan, Y.; Chen, S.; Deng, L.; Duan, Y.; Huang, Z.; Gong, D.; Zhang, G. Construction and characterization of egg white protein-gallic acid-xanthan gum-based emulsion and oleogel. *Food Hydrocoll.* **2024**, *150*, 109720. [CrossRef]
29. Revadekar, C.C.; Godiya, C.B.; Park, B.J. Novel soy protein isolate/sodium alginate-based functional aerogel for efficient uptake of organic dye from effluents. *J. Environ. Manag.* **2024**, *352*, 120011. [CrossRef]
30. Lu, W.; Zhang, C.; Li, Y.; Qin, Z.; Li, X.; Li, Y.; Zhang, K. Double cross-linked chitosan sponge encapsulated with ZrO_2/soy protein isolate amyloid fibrils nanoparticles for the fluoride ion removal from water. *Int. J. Biol. Macromol.* **2024**, *279*, 135520. [CrossRef]
31. Sun, Y.; Li, Y.; Chen, B.; Wang, M.; Zhang, Y.; Chen, K.; Du, Q.; Wang, Y.; Pi, X. Methylene blue removed from aqueous solution by encapsulation of bentonite aerogel beads with cobalt alginate. *ACS Omega* **2022**, *7*, 41246–41255. [CrossRef] [PubMed]
32. Zhou, G.; Zhang, H.; Bai, Z.; Jiang, J.; Wang, Y.; Quan, F. Efficient and rapid adsorption of methylene blue dyes by novel metal-organic frameworks and organic/inorganic hybrid alginate-based dual network gel composites. *Int. J. Biol. Macromol.* **2023**, *253*, 127034. [CrossRef] [PubMed]
33. Su, H.; Deng, T.; Qiu, W.; Hu, T.; Zheng, X.; Peng, K.; Zhang, Y.; Zhao, Y.; Xu, Z.; Lei, H.; et al. One stone, two birds: An eco-friendly aerogel based on waste pomelo peel cellulose for the efficient adsorption of dyes and heavy metal ions. *Int. J. Biol. Macromol.* **2024**, *273*, 132875. [CrossRef] [PubMed]
34. Deng, Y.; Yang, M.; Xiao, G.; Jiang, X. Preparation of strong, tough and conductive soy protein isolate/poly(vinyl alcohol)-based hydrogel via the synergy of biomineralization and salting out. *Int. J. Biol. Macromol.* **2024**, *257*, 128566. [CrossRef] [PubMed]
35. Pasban, A.; Mousavi, S.F.; Abdollahi, S.; Hesarinejad, M.A. Evaluating the potential of soy protein isolate/alginate hydrogel as polyphenolic liposome carrier during gastrointestinal tract: A case study on sumac extract. *LWT Food Sci. Technol.* **2024**, *211*, 116883. [CrossRef]
36. Wang, Z.; Song, L.; Wang, Y.; Zhang, X.; Hao, D.; Feng, Y.; Yao, J. Lightweight UiO-66/cellulose aerogels constructed through self-crosslinking strategy for adsorption applications. *Chem. Eng. J.* **2019**, *371*, 138–144. [CrossRef]
37. Ma, J.; Yu, F.; Zhou, L.; Jin, L.; Yang, M.; Luan, J.; Tang, Y.; Fan, H.; Yuan, Z.; Chen, J. Enhanced adsorptive removal of methyl orange and methylene blue from aqueous solution by alkali-activated multiwalled carbon nanotubes. *ACS Appl. Mater. Interfaces* **2012**, *4*, 5749–5760. [CrossRef]
38. Chen, L.; Zhu, Y.; Cui, Y.; Dai, R.; Shan, Z.; Chen, H. Fabrication of starch-based high-performance adsorptive hydrogels using a novel effective pretreatment and adsorption for cationic methylene blue dye: Behavior and mechanism. *Chem. Eng. J.* **2021**, *405*, 126953. [CrossRef]

39. Aljar, M.A.A.; Rashdan, S.; Abd El-Fattah, A. Environmentally friendly polyvinyl alcohol-alginate/bentonite semi-interpenetrating polymer network nanocomposite hydrogel beads as an efficient adsorbent for the removal of methylene blue from aqueous solution. *Polymers* **2021**, *13*, 4000. [CrossRef]
40. Jiang, R.; Yao, J.; Yao, Y. Optimization of the modified soybean straw activated carbon for adsorption of methylene blue dye by response surface methodology. *Pol. J. Environ. Stud.* **2023**, *32*, 4073–4082. [CrossRef]
41. Shah, S.S.; Ramos, B.; Teixeira, A.C.S.C. Adsorptive removal of methylene blue dye using biodegradable superabsorbent hydrogel polymer composite incorporated with activated charcoal. *Water* **2022**, *14*, 3313. [CrossRef]